AUTHOR(S):

TITLE:

YEAR:

Publisher citation:

OpenAIR citation:

Publisher copyright statement:

This is the _____ version of an article originally published by _____ in _____ (ISSN _____; eISSN _____).

Accepted Manuscript

Gas-condensate flow modelling for shale reservoirs

Ismail Labed, Babs Oyeneyin, Gbenga Oluyemi

Gas-Condensate Flow Modelling for Shale Reservoirs

Ismail Labed, Heriot-Watt University, **Babs Oyeneyin,** Robert Gordon University and **Gbenga Oluyemi,** Robert Gordon University

Abstract

Condensate banking is the most challenging engineering problem in the development of gas-condensate reservoirs where the condensate accumulation can dramatically reduce the gas permeability resulting in impairment of wells productivity. An accurate assessment of condensate banking effect is important to predict well productivity and to diagnose well performance.

Traditionally, Darcy law, combined with relative permeability models, has been used for modelling condensate banking effect in conventional reservoirs. This approach is also widely adopted in reservoir engineering commercial tools. However, for shale gas-condensate reservoirs, the gas flow deviates from Darcy flow to Knudsen flow due to the very small pore size in shale matrix (3-300 nm), compared to conventional reservoirs (10 -200 µm). This gas flow is highly dependent on pore size distribution and reservoir pressure.

In this paper, the effect of condensate saturation on Knudsen flow in shale matrix kerogen is investigated using a 3D pore network with a random pore size distribution. The Knudsen flow is incorporated at the pore level and gas permeability is evaluated for the whole network. In addition, the pore distribution effect in terms of log-normal mean and standard deviation is investigated. The concept of relative permeability in Darcy flow is extended to Knudsen flow by defining a new parameter called relative correction factor ξ_{rel} to evaluate the effect of condensate banking on Knudsen flow. This parameter can be employed directly in reservoir engineering tools.

Simulation results showed that the relative correction factor is not only dependent on condensate saturation but also on pressure. This is due to the impact of pressure on the contribution of pore size ranges into the gas flow. In addition, results showed the effect of the pore size distribution where the standard deviation controls mainly the behaviour of Knudsen flow under condensate saturation. Disregarding this effect can lead to an overestimation of Knudsen flow contribution in well production under condensate banking effect.

Introduction

In the last decade, shale plays emerged as one of the most important oil and gas resources in the world. In 2014, shale gas accounted for 51% of all US natural gas reserves (EIA. 2015). Shale reservoirs are characterised by very small pore size (from 3 to 300 nm) (Williams 2012) and a very low matrix permeability, probably on the order of 10 µD or 100 nD. A horizontal well, combined with hydraulic fracturing, is required to make this type of resources commercially valuable.

The gas-condensate flow in hydrocarbon reservoirs has long been recognized as having the most complex fluid flow dynamics in reservoir engineering (Hinchman and Barree. 1985; Barnum et al. 1995; Du et al. 2004). A condensate buildup can rapidly occur around a producing well when the bottom hole flowing pressure falls below dew-point. The condensate accumulation reduces the gas relative permeability resulting in a brisk decline of well productivity and reduction of heavy components fraction at the wellhead. This phenomenon is usually referred to as "*condensate banking*" or "*condensate blockage*". The condensate banking is controlled by three factors: the flow behaviour, the phase behaviour and the development strategy.

In conventional reservoirs, the condensate banking effect can be reduced by pressure maintenance to be able to produce at a bottomhole pressure above dew point. In shale reservoirs, due to very low permeability, wells start to produce under a bottomhole pressure below the dew point in the few first days or months of production. As no method is available to maintain pressure in shale reservoirs, this type of resources continues to produce under condensate banking effect for the most of the well's life.

For conventional reservoirs, the effect of condensate banking on gas flow is interpreted by using relative permeability models. The apparent gas permeability at a condensate saturation is adjusted using the gas relative permeability as a correction factor. However, in shale reservoirs at the nanopore level, the gas flow deviates from conventional Darcy flow to Knudsen flow. Knudsen flow occurs in nanopores due to the interaction between molecules-molecules and molecules-pore walls resulting in an increasing apparent permeability with decreasing pore size and decreasing pore pressure (Javadpour 2007).

Although the dry gas flow under Knudsen conditions in shale gas reservoirs has been the subject of numerous research studies (Javadpour. 2009; Freeman et al. 2012; Mehmani et al. 2013; Civan. 2010), the effect of multiphase gas-condensate flow is still not well addressed. As Knudsen flow is highly dependent on pore size, the effect of condensate accumulation alters the range of pore sizes that are accessible by gas flow which affects Knudsen flow at the macro-scale level. Therefore, the understanding of how Knudsen flow is affected by condensate banking is essential to evaluate accurately the shale gas-condensate well performance.

Pore-network modelling has become a well-established discipline for petroleum applications for single phase and multiphase flow in porous media. The pore network modelling was first introduced by Fatt (1956). Usually, the void in the porous media is represented by a 2D or 3D network of pores connected by pore throats. The network modelling has been used by researchers to study macroscopic properties of porous media such as permeability and relative permeability by using the pore-level physics of fluid flow and pore space paraments (e.g. pore shapes, wettability and interfacial tension) (Fang et al. 1996; Jamiolahmady et al. 2000; Bustos and Toledo. 2003; Li and Firoozabadi. 2000).

Traditionally, the pores are modelled as spheres or cubes and pore throats are modelled as curved triangular cross-section tubes in conventional reservoirs. A variety of shapes were used in literature, ranging from angular cross-section to grain boundary pores (Blunt. 2001; Joekar-Niasar and Hassanizadeh. 2012). The main challenge of an accurate network modelling is to capture the complexity of the pore space geometry while using simple pore shapes. For multiphase flow, the shapes of pores and pore throats are very important to describe the capillary pressure as a function of wetting phase saturation. When a wetting phase exists in a pore, it occupies the pore corners with high capillary pressure. As saturation increases the capillary pressure decreases until it forms a bridge.

The extension of pore geometry from conventional reservoirs to shale reservoirs should be considered carefully due to the difference of pore space geometry. The shale porosity comprises organic porosity in kerogen and inorganic intergranular porosity. The pore space in organic matter (kerogen) tends to have mainly a round shape which is different from the triangular intergranular shape in conventional sandstone reservoirs(Curtis et al. 2010).

For shale reservoirs, reliable measurement techniques of multiphase permeability are still yet to be developed due to the difficulties related to the control and the measurement of the different phases' saturations in shale matrix samples. Alternatively, pore-network modelling can be used to investigate multiphase flow in shale reservoirs. Mehmani et al. (2013) used single phase gas pore network model to study the effect of Knudsen flow. However, they used an intergranular sandstone pore model. They concluded that the gas apparent permeability is sensible to the fraction of nanopores. Huang et al. (2016) developed a two-phase (gas and water) 3D pore network model including Klinkenberg flow and gas adsorption. Their network

is mixed wettability, organic and non-organic, however, they used a square cross section for pore in kerogen which is not in line with experimental observation where nanopores have circular cross section.

In addition, the high capillary pressure in shale matrix affects the phase behaviour of gas-condensate fluids. The phase behaviour deviation of hydrocarbons in shale reservoirs was studied by many researchers (Brusilovsky 1992; Espósito, Tavares and Castier 2005; Nojabaei, Johns and Chu 2013; Labed, Oyeneyin and Oluyemi 2015) and they concluded that condensate tends to start forming at higher dew point and to reach higher saturations than in conventional reservoirs. This is mainly due the significant lower condensate pressure (created by high capillary pressure) than gas pressure at the pore level. Labed (2016) used Peng-Robinson EoS (Equation of State) combined with Young-Laplace equation to investigate the phase behaviour deviation of gas-condensate fluids in shale matrix with a log-normal pore size distribution. He concluded that the deviation in terms of condensate saturation is about 10% and less than 5% for rich and lean gas-condensate fluids, respectively; however, these results are still needed to be validated by experimental investigations.

This paper presents an investigation of multiphase flow of gas-condensate fluids in shale matrix using a simple pore network modelling with a focus on the impact of condensate banking on Knudsen flow assuming a limited effect of phase behaviour deviation due to the capillary pressure and gas adsorption. In this research project, the modelling of phase behaviour deviation of gas-condensate in shale matrix and its effect on Knudsen flow have been investigated and results will be presented in a future paper.

Gas Flow in Nanopores

Shale reservoirs are dual porosity/dual permeability systems containing two media: matrix and fractures network (including natural fractures and hydraulically induced fractures). The fluid flows from matrix to the fracture and then to the wellbore. The matrix plays two roles; fluid storage and conductivity to the fractures while fractures serve as connection between matrix and the wellbore. While the fluid flow in fractures in shale reservoirs is similar as in conventional reservoirs, it is commonly believed that the existence of an extensive networks of natural fractures is essential to for a successful hydraulic fracturing (Forand et al. 2017; Walton and McLennan. 2013). The main difference of fluid dynamics between shale reservoirs and conventional reservoir resides in shale matrix where Darcy law fails to describe the gas flow in pores at nano and micro-scale.

Three non-Darcy flow regimes: slip flow, transition flow and free-molecular flow can be distinguished using Knudsen number which is defined as a measure of the degree of density rarefaction of gas flow in micro and nano-channels (Karniadakis et al. 2005). It is mathematically expressed as:

$$Kn = \frac{\lambda}{R} \qquad (1)$$

where R is the hydraulic radius (m) and λ is the average minimum free path (m), defined as

$$\lambda = \frac{\mu Z}{P} \sqrt{\frac{\pi R_g T}{2M}} \qquad (2)$$

where μ is the viscosity (Pa.s), Z is the compressibility factor, P is the absolute gas pressure (Pa), T is the absolute temperature (K), M is the average molecular mass (kg/kmol) and Rg is the universal gas constant.

Table 1 and Fig. 1 illustrate the classification of flow conditions according to the Knudsen number limits in pipes as the continuum, slip, transition and free molecular flow regimes (Karniadakis et al. 2005).

Table 1—Classification of flow conditions in pipes according to the Knudsen number limits (Karniadakis et al. 2005)

Knudsen number	$Kn < 0.01$	$0.01 < Kn < 0.1$	$0.1 < Kn < 10$	$Kn > 10$
Flow regime	Continuum	Slip	Transition	Free molecular

Continuum flow occurs at *Kn* values under 0.01 where molecule-molecule interaction is the dominant force. Hagen–Poiseuille law describes continuum flow in channels as

$$q = \frac{\pi}{8} \frac{R^4 \Delta P}{\mu L} \tag{3}$$

where q is fluid rate, R is the radius of the channel in m (m³/s), ΔP is pressure difference (Pascal), μ is the fluid viscosity (cp) and L is the channel length (m).

At $0.01 < Kn < 0.1$ range the molecule-wall effect is more pronounced, but molecule-molecule interaction is still dominant. Slip flow regime dominates when gas molecules near to the channel walls don't exhibit a zero velocity (slip). Navier-Stokes equation is still valid to describe this flow regime with a velocity discontinuity at channel walls. Klinkenberg (1941) model is routinely used to correct permeability measurement in gas core flooding at laboratory conditions.

Transition flow occurs with increasing Kn numbers $0.1 < Kn < 10$) translated by a transition from slip flow to free molecular flow. At this range of Kn, traditional flow dynamics laws start to break down.

In free molecular flow, the molecule-wall interaction is dominant when the average minimum free path is much higher than the channel radius ($\lambda \gg R$). Molecules are more likely to collide with the channel wall than colliding with other molecules. Fig. 1 summaries the flow regimes according to Knudsen number.

Different Knudsen number limits were suggested by some researchers for flow regime classification. Roy et al. (2003) and Javadpour (2009) recommended 0.001 for the lower limit of Knudsen number for slip flow instead of 0.01 proposed by Karniadakis et al. (2005). Nevertheless, the results presented in this work are independent of Knudsen number limits used for flow regime classification.

Using Direct-simulation of Monte Carlo (DSMC) and Linearized Boltzmann solution (LBS) results, Beskok and Karniadakis (1999) proposed a general flow model that covers all gas flow regimes in micro channels using a correction factor ξ where

$$\xi = (1 + \alpha K_n)(1 + \frac{4K_n}{1 - bK_n}) \tag{4}$$

Therefore, Hagen–Poiseuille equation can be modified as

$$q = \xi \frac{\pi}{8} \frac{R^4 \Delta P}{\mu L} \tag{5}$$

Where α is the dimensionless rarefaction coefficient, and b is the empirical slip coefficient independent of the gas properties that can be determined experimentally or using direct-simulation Monte Carlo (b = -1 for fully-developed slip flow through channels and tube).

Beskok and Karniadakis (1999) used Loyalka and Hamoodi (1990) experimental data and proposed the following correlation of the rarefaction coefficient α in function of Knudsen number

$$\alpha = \frac{128}{15 \pi^2} (4 K_n^{0.4}) \tag{6}$$

4

Fig. 2 illustrates an example of the correction factor for methane as a function of pore radius at different pressure values and it indicates that Knudsen flow increases with decreasing pore radius and decreasing pressure.

The effect of liquid saturation on gas slip flow is well documented in the literature. Rose (1948) carried out gas–water core flooding experiments using synthetic materials and natural sandstone samples with intrinsic permeabilities ranging from 30 mD to 800 mD (which is considered as conventional reservoirs) and he found that the slippage effect decreases with increasing water saturation. Estes and Fulton (1956) and Sampath and Keighin (1982) used similar range of sandstone permeabilities and reported similar observations. Rushing, Newsham and Fraassen (2003) extended Rose' work to tight gas reservoir using sandstone cores with permeability ranging from 0.01 to 0.1 mD leading to the validation of the effect of water saturation on slippage effect in tight reservoirs.

Estes and Fulton (1956) explained the effect of water saturation on gas slippage effect by the variation of pore size range that is accessible for gas flow as the water saturation increases. Due to capillary forces, when water saturation increases it occupies the smallest free pore size range, hence increasing the average pore size accessible by gas flow which reduces the gas slippage effect.

Recently, Wu et al.(2014) used a synthetic material to build a 1D nanoscale slit-like channels with 100 nm size to describe gas-water flow in shale matrix. However, their results were not in agreement with the conclusions of Rose (1948), Sampath and Keighin (1982) and Rushing et al. (2003); they found that gas slippage effect increases as the water saturation increases. The main reason behind this result is that their 1D nano-channel network does not reflect the pore interaction and the pore size variation as in shale, tight sandstones and conventional sandstone core samples used by other researchers. Thus, the variation of pore size accessible by gas with increasing water saturation is not represented in their work.

Condensate flow in shale matrix, just like general liquids flow in nano-scale, is still a very active subject in material science. Among the research community, a liquid flow is always a continuum flow governed by Hagen–Poiseuille equation as the rarefaction effect doesn't extend to liquid phase (Mattia and Gogotsi. 2008). Many researchers emphasised the similarity of the slug flow of gas-liquid fluids between microscale and nanoscale (Günther and Jensen. 2006; Gogotsi et al. 2000). Experimental studies of hydrocarbon fluids (e.g. gas-condensate fluids) flow in nanotube have not been reported in the literature.

Pore Network Modeling

Description of the Pore Space. From the literature, a number of experiments were reported on the application of Mercury Injection Capillary Pressure technique (MCIP) to determine the pore size distribution (Lewis, et al. 2013, Kuila 2013, Saidian 2014, Ross and Bustin 2009, Al Hinai et al. 2014, Crousse, et al. 2015). Fig. 3 represents the incremental pore space fraction vs. pore radius for four samples from Eagle Ford Shale (adapted from Lewis, et al.(2013)). In this figure, pore radius extends from 3nm up to 300 nm with a logarithmic bell-shape around 10 to 40 nm which can be approximated to a log normal distribution. Fig.4 shows an approximation of Lewis, et al. (2013) data (Sample 4) to a log normal distribution of a mean $v=6$ and standard deviation $s=0.6$ i.e. $\ln \mathcal{N}(v = 10, s = 0.6)$.

In this study, porous media in shale matrix is modelled as three-dimensional cubic network of connected pore segments and nodes are concocted to have infinite connectivity. Each pore segment connecting nodes i and j is modelled as nanotubes with radial cross section of radius R_{ij} and constant length L (see Fig. 5). Nanotubes' radii are assigned randomly following a log-normal distribution $\ln \mathcal{N}(v, s)$. Fig. 6 illustrates an 8×8×8 pore network structure with connection number $Z= 6$. Fig. 7 shows the pore radius distribution of $\ln \mathcal{N}(10, 0.6)$ network and the theoretical log normal PDF used to generate it randomly. The dimension in X, Y and Z direction is 1 µm and the porosity is 0.08.

The PDF (Probability Density Function) for R is written as

$$f(R) = \frac{\sqrt{2}\exp\left[-\frac{1}{2}\left(\frac{\ln R - \ln v}{s}\right)^2\right]}{\sqrt{\pi}\, s\, R\left[\text{erf}\left(\frac{\ln R_{max} - \ln v}{\sqrt{2}s}\right)\text{erf}\left(\frac{\ln R_{min} - \ln v}{\sqrt{2}s}\right)\right]} \tag{7}$$

Table 2 presents a gas condensate composition sample used to generate the CVD (Constant Volume Depletion) liquid drop-out and Interfacial tension (IFT) presented in Fig. 8 using a commercial PVT software (ECLIPSE PVTi). The sample can be defined as medium-rich gas condensate fluid with maximum liquid dropout of 22% and dew point of 4250 psi. The CVD experiment mimics the fluid flow in shale reservoir where only gas is expected to flow in the two-phase region.

Table 2— Gas condensate sample composition used in calculation

Components	Mol. Fraction (%)	Mol. Weight	Spec. Gravity
C1	70	16.0	
C2	9	30.1	
C3	6	44.1	
C4	6	58.1	
C5	2	72.2	
C6	1	84.0	
C7+	6	167	0.8122

As pressure drops, condensate builds up in the pore network and starts to fill up the small pores. Due to the high capillary pressure, all pores lower than the minimum free pore for gas flow $R_{g,min}$ is considered to be blocked by condensate.

A volume function is used to calculate $R_{g,min}$ as a function of condensate saturation S_c based on the pore distribution and volumes (see Equation 8).

$$R_{g,min} = f(S_c) \tag{8}$$

where $R_{g,min}$ and S_c can be related in discretised version as:

$$S_c(R_{g,min}) = \frac{\sum_{R_{min}}^{R_{g,min}} R_{ij}^2}{\sum_{R_{min}}^{R_{max}} R_{ij}^2} \tag{9}$$

Fig. 9 illustrates the results of generated $R_{g,min}$ as function of condensate saturation S_c of the pore network while Fig. 10 represents an example of pore network with pores filled by condensate in red and pores filled by gas in green at maximum condensate saturation of 22%.

Condensate Trapping. To investigate the effect of capillary pressure, two nanotube T_1 and T_2 with radii R_1 and R_2, respectively were adopted for analysis (see Fig. 11) where condensate is present in *Tube 1*. The condensate will flow to *Tub2 2* if

$$\Delta P = P_{liq,1} - P_{liq,2} > 0 \tag{10}$$

where $P_{vap,1}$ and $P_{vap,2}$ are gas pressure in Tube1 and Tube2 respectively and they can be expressed as

$$P_{liq,i} = P_{vap,i} - P_{cap,i} \qquad i = 1,2 \tag{11}$$

Condition (10) can be rewritten as

$$P_{vap,1} - P_{vap,2} > P_{cap,1} - P_{cap,2} \tag{12}$$

where $P_{cap,1} - P_{cap,2}$ is defined as the differential pressure threshold ΔP_{thr} for the condensate to flow from *Tube 1* to *Tube 2*

$$\Delta P_{thr} = P_{cap,1} - P_{cap,2} = \sigma_{gl} \, cos\theta \left(\frac{1}{R_1} - \frac{1}{R_2} \right) \tag{13}$$

For the pore network defined previously, ΔP_{thr} was calculated numerically for each nanotube for the condensate to flow to the neighbouring larger radius nanotube at different reservoir pressure values: 60, 500, 3000 and 4200 psi. Results are shown in Fig. 12.

To compare ΔP_{thr} to pressure values applied on shale matrix in the field, a maximum reservoir pressure of 8000 psi, a minimum bottomhole pressure of 500 psi and a minimum shale matrix dimension of 10×10×100 ft are considered which result to a maximum differential drainage pressure ΔP_D of 3E-3 psi. Comparing levels of ΔP_{thr} (see Fig. 12) to the maximum differential drainage pressure in the field ΔP_D, one can conclude that gas cannot displace condensate i.e. condensate is trapped by capillary pressure and all nanotubes with condensate saturation can be considered blocked.

Furthermore, ΔP_{thr} increases with decreasing reservoir pressure. Consequently, the condensate trapping mechanism is expected to be more pronounced around wellbore than in deep reservoir as the pressure decreases from the reservoir to the wellbore.

Flow Modelling. The gas flow through nanotubes connecting two nodes *i* and *j* is described by the modified Hagen-Poiseuille equation (3) as

$$\Delta P_{ij} = \begin{cases} \dfrac{1}{\xi_{ij}} \left[\dfrac{8}{\pi} \, \dfrac{\mu_{ij}^g \, L_{ij} \, q_{ij}^g}{R_{ij}^4} \right] \text{ for gas} \\[4mm] \left[\dfrac{8}{\pi} \, \dfrac{\mu_{ij}^c \, L_{ij} \, q_{ij}^c}{R_{ij}^4} \right] \text{ for condensate} \end{cases} \qquad i = 1..N, j = 1..N \tag{14}$$

where q_{ij} is phase flow rate (l/s), ΔP_{ij} is differential pressure (Pa), R_{ij} is tube radius (m), μ_{ij} is phase viscosity (Pa.s) and L_{ij} is tube length (m), superscripts g and c stand for gas and condensate, respectively. The gas permeability correction factor of individual nanotube ξ_{ij} is defined as

$$\xi_{ij} = \left(1 + \alpha_{ij} Kn_{ij} \right) \left(1 + \frac{4Kn_{ij}}{1 - Kn_{ij}} \right) \qquad i = 1..N, j = 1..N \tag{15}$$

where Kn_{ij} is the nanotube's Knudsen number defined in Equation (1).

A nanotube conductivity for gas is defined as

$$G_{ij}^g = \frac{q_{ij}^g}{\Delta P_{ij}} = \xi_{ij} \frac{\pi R_{ij}^4}{8 \, \mu_{ij}^g \, L_{ij}} \qquad i = 1..N, j = 1..N \tag{16}$$

and for condensate

$$G_{ij}^c = \frac{q_{ij}^c}{\Delta P_{ij}} \equiv \frac{\pi R_{ij}^4}{8\, \mu_{ij}^c\, L_{ij}} \quad i = 1..N, j = 1..N \tag{17}$$

The gas flow through the pore network is governed by mass conservation of gas and condensate in each node (i, j)

$$\sum_{j=1}^{N} q_{ij}^g = 0 \ \text{ and } \ \sum_{j=1}^{N} q_{ij}^c = 0 \quad i = 1..N \tag{18}$$

Equation (18) can be written using Equation (16) as

$$\sum_{j=1}^{N} G_{ij}^g\, \Delta P_{ij} = 0 \ \text{ and } \ \sum_{j=1}^{N} G_{ij}^c\, \Delta P_{ij} = 0 \quad i = 1..N \tag{19}$$

Replacing ΔP_{ij} by $P_i - P_j$ gives

$$P_i \sum_{j=1}^{N} G_{ij}^g - \sum_{j=1}^{N} G_{ij}^g\, P_j = 0 \ \text{ and } \ P_i \sum_{j=1}^{N} G_{ij}^c - \sum_{j=1}^{N} G_{ij}^c\, P_j = 0 \quad i = 1..N \tag{20}$$

A code was written in Matlab using iterative Newton-Raphson method for unknown vector P_i to solve Equation (20), to generate the 3D pore network and to calculate volumetric functions. The flow diagram of the code is presented in

Fig. 13.

Network Gas Apparent Permeability and Relative Correction Factor Calculation. The apparent permeability and gas Darcy permeability of the pore network are calculated respectively as

$$k_{app} = \frac{q_{app}\, \mu_{avg}\, L}{P_i - P_o} \tag{21}$$

and

$$k_D = \frac{q_D \mu_{avg} L}{P_i - P_o} \tag{22}$$

where μ_{avg} is the pore network average viscosity, L is the pore network dimension in flow direction and P_i and P_o are inlet and outlet pressure, respectively.

The enhancement factor is calculated as:

$$\xi = \frac{k_{app}}{k_D} \tag{23}$$

To emphasise the effect of condensate blockage on correction factor, gas condensate correction factor ξ_{GC} and dry gas correction factor ξ_{DG} are calculated as

$$\xi_{GC} = \frac{k_{app,GC}}{k_{D,GC}} \quad \text{ and } \quad \xi_{DG} = \frac{k_{app,DG}}{k_{D,DG}} \tag{24}$$

8

where $k_{app,GC}$ and $k_{D,GC}$ are apparent Knudsen permeability and Darcy permeability with condensate blockage, respectively. $k_{app,DG}$ and $k_{D,DG}$ are apparent Knudsen permeability and Darcy permeability of dry gas, respectively.

In order to evaluate the effect of condensate saturation on Knudsen flow, a new parameter is defined as "Relative Correction factor" ξ_{rel} which is the ratio of ξ_{GC} to ξ_{DG}

$$\xi_{rel} = \frac{\xi_{GC}}{\xi_{DG}} \tag{25}$$

ξ_{rel} is a measure of the effect of condensate blockage on Knudsen flow and it can be used to adjust correction factor from dry gas flow to gas condensate flow. ξ_{rel} for Knudsen flow can be perceived as the equivalent of gas relative permeability k_{rg} for Darcy flow.

So, the gas apparent permeability at the presence of condensate in shale matrix can be calculated as a function of intrinsic permeability k_∞, gas relative permeability k_{rg}, correction factor ξ_{DG} and relative correction factor ξ_{rel}. This relationship is presented in Equation (26).

$$k_{app} = \xi_{rel}\ \xi_{DG}\ k_{rg}\ k_\infty \tag{26}$$

Numerical Simulations and Results

Using the pore network model, three numerical simulations were carried on:

a) Darcy flow where $\xi_{ij} = 1$

b) Knudsen flow with condensate blockage effect using $R_{g,min}$ defined by Equation (8)

c) Knudsen flow for dry gas: where gas permeability is calculated without condensate blockage. In this experiment, the same gas PVT data of CVD are used for viscosity, Z-factor and molecular weight.

Effect of Condensate Saturation on Gas Apparent Permeability. The results of Darcy relative permeabilities of gas and condensate are presented in Fig. 14. Despite the simplicity of the pore network, the relative permeability results are similar to gas-liquid permeability reported in tight sands by Cluff and Byrnes (2010). The gas permeability declines rapidly as the condensate saturation increases to reach a very low critical saturation of 28% while the condensate remains immobile to very low relative permeability in this range. This result indicates the severity of condensate banking effect on shale gas well deliverability.

The permeability results for the three simulations carried out using an 8×8×8 network with $\ln \mathcal{N}(10, 0.6)$ pore size distribution are presented in a log-log plot in Fig. 15. The change in Darcy permeability reflects the effect of condensate blockage on gas flow below the dew point. The permeability reduction is caused by the loss of permeability of tubes with radius less than $R_{g,min}$. Knudsen permeability plot shows a similar decline below dew point but an enhanced permeability with decreasing pressure where Knudsen flow is more important. In addition, Knudsen dry gas permeability (without condensate blockage) is plotted against Knudsen permeability (with condensate blockage). Fig. 16 compares the correction factor ξ_{GC} under condensate blockage effect with the dry gas correction factor ξ_{DG}. The difference between ξ_{GC} and ξ_{DG} is caused by the loss of the contribution of the small pores with $R_{ij} < R_{g,min}$ to Knudsen flow.

ξ_{rel} is illustrated as a function of pressure in Fig. 17. When pressure drops below dew point, ξ_{rel} starts to decrease reflecting the reduction of Knudsen flow in pores with condensate blockage. The smaller pore radius (blocked with condensate) have an increasing contribution to the total Knudsen flow with decreasing pressure which explains the decline of ξ_{rel}. In this example ξ_{rel} reaches a lower value of 0.87 at 14.7 psi. The rapid decline of ξ_{rel} from 1 to 0.96 just under dew point pressure is due to

the blockage of the smaller pores with the rapid increase of condensate saturation (see Fig. 8). The effect of condensate blockage should be considered in correction factor calculation in order not to overestimate the apparent gas permeability in shale matrix.

To investigate the relationship between condensate saturation, pressure and ξ_{rel}, the simulation was carried out at different pressure values: 14.7, 100, 500, 1000 and 2000 psi. At each reservoir pressure value, the condensate saturation extended (beyond the unique value of CVD) to range from 0 to maximum drop out of 22% and results are given in

Fig. 18. This figure shows that at the same pressure ξ_{rel} decreases with increasing condensate saturation which can be explained by the blockage of the lower part of pores range, hence reducing the effect of Knudsen flow. In addition, this relationship between condensate saturation and ξ_{rel} is affected by pressure as well. The lower the pressure the higher the effect of condensate saturation on ξ_{rel}.

With the purpose of evaluating the contribution of the different pore size ranges and how it affects ξ_{rel}, two parameters are introduced: Class Contribution (CC) C_m^δ and Relative Change of Contribution (RCC) ΔC_m. The pore size distribution is divided into 100 pore size classes and contribution of each class (m) is expressed as a function of pressure; C_m^δ in the dry gas flow was calculated for Darcy flow and Knudsen flow using Equation (28).

$$C_m^\delta(P) = \frac{\sum_{i,j}[q_{ij}^g]}{\frac{\sum_{j=1}^{N}\left(\sum_{j=1}^{N} abs\left[q_{ij}^g\right]\right)}{2}} , tube\ (i,j) \in C_m , m = 1..100 \tag{27}$$

where δ= D or Kn, refers to the flow type: Darcy flow or Knudsen flow, respectively. The relative change of Class Contribution ΔC_m is calculated using Equation (28).

$$\Delta C_m(P) = \frac{C_m^{Kn}(P) - C_m^D(P)}{C_m^D(P)} , m = 1..100 \tag{28}$$

ΔC_m is a measure of the contribution variation of each pore size class with pressure.

The contribution of pore radius ranges to the total gas flow rate for Knudson dry gas simulation C_m^{Kn} at 2200 psi is shown in Fig. 19a while Fig. 19b shows the relative change of this contribution ΔC_m for different pressure values (14.7 100, 500, 1000 and 2200 psi). These figures depict the increase of the contribution of the lower range of pore size. The contribution pattern shifts with pressure i.e. at low pressure (250, 60 and 14.7 psi) lower pore sizes (under 12nm) contribute more than at high pressure (1000 and 2000 psi). When these pores are blocked, the correction factor ξ_{GC} decreases as a function of decreasing pressure, reflecting the loss of Knudsen flow contribution of these pores.

As a result, the Knudsen flow under condensate banking effect can be expressed as a function of by both condensate saturation and reservoir pressure using the relative correction factor

$$\xi_{rel} = f(S_c, P) \tag{29}$$

The saturation controls the range of pore sizes accessible by gas flow and the pressure affects the contribution of these pore sizes to the total Knudsen flow. Using the results generated in this work, the following formulation of ξ_{rel} was derived

$$\xi_{rel} = 1 - \frac{a}{P^b} (S_c)^n \tag{30}$$

where n, a and b are parameters controlled by the pore size distribution. For data used in this work, the estimated values for these parameters are shown in Table 3. Fig. 20 shows ξ_{rel} values from correlation in Equation (30) plotted against values obtained from simulations with R^2=92%.

Table 3— Estimated values of ξ_{rel} parameters for data used in this work

Parameter	Value
n	0.927
a	2.371
b	0.193

ξ_{rel} **Sensitivity to Pore Size Distribution Parameters.** In order to evaluate the effect of pore size distribution, the previous simulations were performed for varying pore mean radius and standard deviation.

8 pore networks with mean pore radius varying from 5 to 30 nm and constant standard deviation of 0.6 were generated randomly to evaluate the effect of the mean value and results in terms of ξ_{rel} vs pressure are shown in Fig. 21 . The effect of condensate blockage decreases with increasing pore mean radius. At higher mean values, small blocked pore sizes have very low contribution to total Knudsen flow. As the mean decreases, the pore size distribution shifts to upper levels which reduces the effect of Knudsen flow in the lower part of radii of the distribution.

Other pore networks with standard deviation varying from 0.1 to 0.8 and constant pore mean radius of 10nm were generated randomly to evaluate the effect of the standard deviation. Results are presented in Fig. 22. The standard deviation reflects the degree of the dispersion of pore radii. At low standard deviation values, pore radii are concentrated around the mean value which leads to an insignificant variation of pore radius range filled by condensate and thus a lower effect on ξ_{rel}. Inversely, at high standard deviation values, the pore size distribution is more dispersed leading to a more significant effect on ξ_{rel}.

In both Fig. 21 and Fig. 22, the fact that some of ξ_{rel} curves cross each other can be explained by the different pore networks generated randomly (in terms of pore radii and their spatial distribution in the network) by the Matlab code for each combination of mean and standard deviation which leads of slightly different ξ_{rel} patterns.

Another sensitivity of ξ_{rel} in terms of connection number Z was carried out with Z values ranging from 6 to 4. The simulations were performed starting with a pore network of Z=6 and connection were removed randomly and progressively to achieve Z values of 5.6, 5.2, 4.8, 4.4 and 4. Results showed in Fig. 23 exhibit a general decreasing of ξ_{rel} with decreasing Z which can be explained by the increasing effect of the lower range of pore sizes due to flow restriction with decreasing Z values.

These results illustrate the importance of describing the shale matrix using pore size distribution rather than single pore radius to be able to estimate the impact of condensate accumulation on the apparent gas permeability.

Conclusions

A more accurate modelling is needed for gas condensate two-phase flow in shale matrix at pore level which takes into consideration pore distribution in pore network and the effect of condensate accumulation on Knudsen flow.

Single pore size models cannot be used to describe Knudsen flow in shale matrix when condensate forms due to the change of the pore size range which is available for gas flow as a function of condensate saturation.

For gas condensate systems, the evaluation of Knudsen flow using pore network models is essential to implement:

a) the changing flow contribution of pore sizes as a function of pressure: at reservoir pressure under 1000 psi lower pore sizes contribute to total gas flow more than at pressure above 1000 psi.

b) the condensate banking effect by eliminating the contribution of lower pore sizes blocked by condensate and its effect on the gas flow in connected higher pore sizes.

A new parameter was introduced in this study, "Relative Correction Factor" ξ_{rel} defined as the ratio of of ξ_{GC} to ξ_{DG}. It is a measure of the effect of condensate blockage on Knudsen flow and it can be used to adjust correction factor from dry gas flow to gas condensate flow.

Results showed that a significant reduction of Knudsen flow effect is observed at high condensate saturation and low reservoir pressure i.e. ξ_{rel} is a function of condensate saturation and pressure. The effect of condensate blockage is highly dependent on the pore size distribution parameters. High values of standard deviation have relatively high condensate blockage effect on Knudsen flow.

The assumption of a constant mean effective pore size with pressure in gas apparent permeability calculation in shale matrix with condensate banking can result in an overestimation of Knudsen flow contribution to well productivity. Considering the effect of condensate saturation on Knudsen flow in well production prediction is essential in order not to overestimate the gas condensate shale recovery.

References

Al Hinai, A., Rezaee, R., Esteban, L. et al. 2014. Comparisons of pore size distribution: a case from the Western Australian gas shale formations. *Journal of Unconventional Oil and Gas Resources* **8**: 1-13.

Barnum, R., Brinkman, F., Richardson, T. et al. 1995. Gas condensate reservoir behaviour: productivity and recovery reduction due to condensation. Presented at the SPE Annual Technical Conference and Exhibition.

Beskok, A. and Karniadakis, G.E. 1999. Report: a model for flows in channels, pipes, and ducts at micro and nano scales. *Microscale Thermophysical Engineering* **3** (1): 43-77.

Blunt, M.J. 2001. Flow in porous media—pore-network models and multiphase flow. *Current opinion in colloid & interface science* **6** (3): 197-207.

Brusilovsky, A.I., 1992. Mathematical simulation of phase behavior of natural multicomponent systems at high pressures with an equation of state. *SPE reservoir engineering,* 7(1): 117-122

Bustos, C.I. and Toledo, P.G. 2003. Pore-level modeling of gas and condensate flow in two-and three-dimensional pore networks: Pore size distribution effects on the relative permeability of gas and condensate. *Transport in Porous Media* **53** (3): 281-315.

Civan, F. 2010. A review of approaches for describing gas transfer through extremely tight porous media. Presented at the AIP Conference Proceedings.

Cluff, R.M. and Byrnes, A.P. 2010. Relative Permeability In Tight Gas Sandstone Reservoirs-The" Permeability Jail" Model. Presented at the SPWLA 51st Annual Logging Symposium.

Crousse, L.C., Cuervo, S.A., Vallejo, D. et al. 2015. Unconventional Shale Pore System Characterization in El Trapial Area, Vaca Muerta, Argentina.

Curtis, M.E., Ambrose, R.J. and Sondergeld, C.H. 2010. Structural characterization of gas shales on the micro-and nano-scales. Presented at the Canadian Unconventional Resources and International Petroleum Conference.

Du, Y., Guan, L. and Bai, B. 2004. Well Deliverability Loss Analysis in the Gas Condensate Reservoir. Presented at the Canadian International Petroleum Conference.

EIA 2015. U.S. Crude Oil and Natural Gas Proved Reserves. , https://www.eia.gov/naturalgas/crudeoilreserves/.

Espósito, R., Tavares, F. and Castier, M., 2005. Phase equilibrium calculations for confined fluids, including surface tension prediction models. *Brazilian Journal of Chemical Engineering,* 22(1): 93-104

Estes, R.K. and Fulton, P.F. 1956. Gas slippage and permeability measurements. *Journal of Petroleum Technology* **8** (10): 6973.

Fang, F., Firoozabadi, A., Abbaszadeh, M. et al. 1996. A Phenomenological modeling of critical condensate saturation. Presented at the SPE Annual Technical Conference and Exhibition.

Fatt, I. 1956. The network model of porous media. 2. Dynamic properties of a single size tube network. *Transactions of the American institute of mining and metallurgical engineers* **207** (7): 160-3.

Firincioglu, T., Ozkan, E. and Ozgen, C., 2012. Thermodynamics of Multiphase Flow in Unconventional Liquids-Rich Reservoirs. In: *SPE Annual Technical Conference and Exhibition.*

Freeman, C., Moridis, G., Michael, G. et al. 2012. Measurement, Modeling, and Diagnostics of Flowing Gas Composition Changes in Shale Gas Wells. Presented at the SPE Latin America and Caribbean Petroleum Engineering Conference.

Gogotsi, Y., Libera, J.A. and Yoshimura, M. 2000. Hydrothermal synthesis of multiwall carbon nanotubes. *Journal of Materials Research* **15** (12): 2591-4.

Günther, A. and Jensen, K.F. 2006. Multiphase microfluidics: from flow characteristics to chemical and materials synthesis. *Lab on a Chip* **6** (12): 1487-503.

Hinchman, S. and Barree, R. 1985. Productivity loss in gas condensate reservoirs. Presented at the SPE Annual Technical Conference and Exhibition.

Huang, X., Bandilla, K.W. and Celia, M.A. 2016. Multi-Physics Pore-Network Modeling of Two-Phase Shale Matrix Flows. *Transport in Porous Media* **111** (1): 123-41.

Jamiolahmady, M., Danesh, A., Tehrani, D. et al. 2000. A mechanistic model of gas-condensate flow in pores. *Transport in Porous Media* **41** (1): 17-46.

Javadpour, F., Fisher, D. and Unsworth, M., 2007. Nanoscale gas flow in shale gas sediments. Journal of Canadian Petroleum Technology, 46(10).

Javadpour, F. 2009. Nanopores and apparent permeability of gas flow in mudrocks (shales and siltstone). *Journal of Canadian Petroleum Technology* **48** (8): 16-21.

Joekar-Niasar, V. and Hassanizadeh, S. 2012. Analysis of fundamentals of two-phase flow in porous media using dynamic pore-network models: a review. *Critical Reviews in Environmental Science and Technology* **42** (18): 1895-976.

Klinkenberg, L. 1941. The permeability of porous media to liquids and gases. Presented at the Drilling and production practice.

Karniadakis, G., Beskok, A. and Aluru, N., Microflows and nanoflows: fundamentals and simulation. 2005.

Kuila, U. 2013. Measurement and interpretation of porosity and pore-size distribution in mudrocks: The hole story of shales: Colorado School of Mines.

Labed, I., Oyeneyin, B. and Oluyemi, G., 2015, September. Hydraulic Fracture Spacing Optimisation for Shale Gas-Condensate Reservoirs Development. In SPE Offshore Europe Conference and Exhibition. Society of Petroleum Engineers.

Labed, I. 2016. Gas-condensate flow modelling for shale gas reservoirs. Robert Gordon University, PhD thesis.

Lewis, R., Singer, P., Jiang, T. et al. 2013. NMR T2 distributions in the Eagle Ford shale: Reflections on pore size. Presented at the SPE Unconventional Resources Conference-USA.

Li, K. and Firoozabadi, A. 2000. Phenomenological modeling of critical condensate saturation and relative permeabilities in gas/condensate systems. *SPE Journal* **5** (02): 138-47.

Loyalka, S. and Hamoodi, S. 1990. Poiseuille flow of a rarefied gas in a cylindrical tube: solution of linearized Boltzmann equation. *Physics of Fluids A: Fluid Dynamics (1989-1993)* **2** (11): 2061-5.

Mattia, D. and Gogotsi, Y. 2008. Review: static and dynamic behavior of liquids inside carbon nanotubes. *Microfluidics and Nanofluidics* **5** (3): 289-305.

Mehmani, A., Prodanović, M. and Javadpour, F. 2013b. Multiscale, multiphysics network modeling of shale matrix gas flows. *Transport in Porous Media* **99** (2): 377-90.

Nojabaei, B., Johns, R.T. and Chu, L., 2013. Effect of capillary pressure on phase behavior in tight rocks and shales. *SPE Reservoir Evaluation & Engineering,* 16(03): 281-289

Rose, W.D. 1948. Permeability and gas-slippage phenomena. *28 th Annual Mtg.Topical Committee on Production Technology* .

Ross, D.J. and Bustin, R.M. 2009. The importance of shale composition and pore structure upon gas storage potential of shale gas reservoirs. *Marine and Petroleum Geology* **26** (6): 916-27.

Roy, S., Raju, R., Chuang, H.F. et al. 2003. Modeling gas flow through microchannels and nanopores. *Journal of Applied Physics* **93** (8): 4870-9.

Rushing, J., Newsham, K. and Fraassen, K. 2003. Measurement of the two-phase gas slippage phenomenon and its effect on gas relative permeability in tight gas sands. Presented at the SPE Annual Technical Conference and Exhibition.

Saidian, M. 2014. Porosity and pore size distribution in mudrocks: a comparative study for Haynesville, Niobrara, Monterey, and Eastern European Silurian Formations.

Sampath, K. and Keighin, C.W. 1982. Factors affecting gas slippage in tight sandstones of cretaceous age in the Uinta basin. *Journal of Petroleum Technology* **34** (11): 2,715,2,720.

Walton, I. and McLennan, J., 2013, May. The role of natural fractures in shale gas production. In *ISRM International Conference for Effective and Sustainable Hydraulic Fracturing*. International Society for Rock Mechanics and Rock Engineering.

Williams, K.E., 2012. PS The Permeability of Overpressure Shale Seals and of Source Rock Reservoirs is the Same. http://www.searchanddiscovery.com/pdfz/documents/2012/40935williams/ndx_williams.pdf.html.

WU, Q. et al., 2014. Optic imaging of two-phase-flow behavior in 1D nanoscale channels. *SPE Journal*, *19(05)*, pp. 793-802

Figures
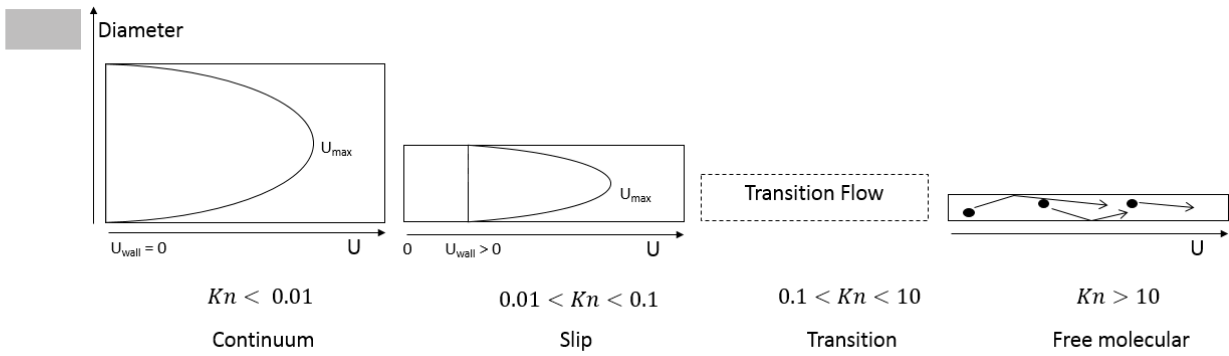
Fig. 1: Different gas flow regimes as function of Knudsen number (not to scale, adapted from Javadpour (2009))
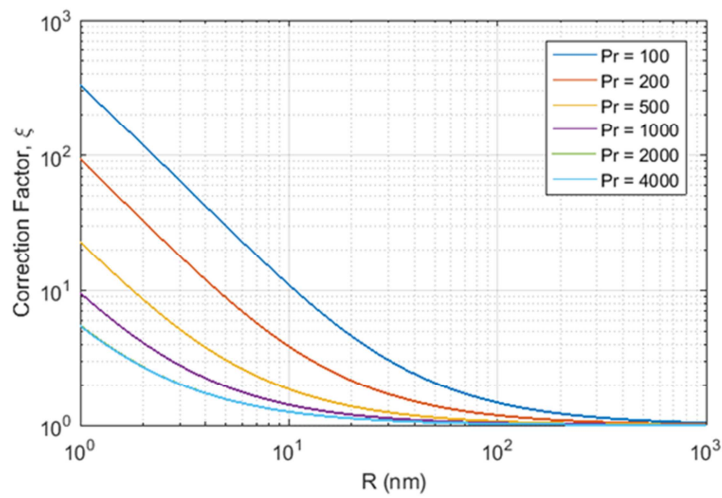
Fig. 2—Log-log of correction factor vs pore radius for different pressure values.
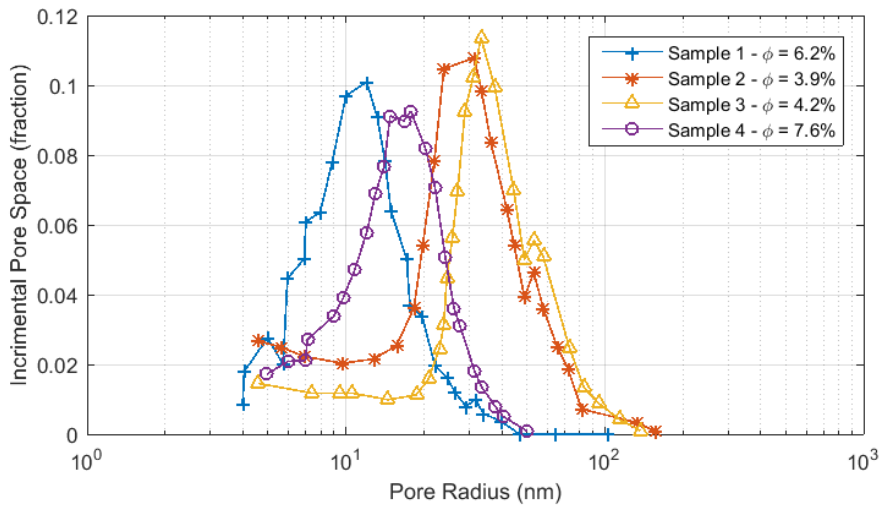
Fig. 3: Incremental pore space vs. pore radius of four samples of lower Eagle Ford Shale (adapted from Lewis, et al. (2013)).
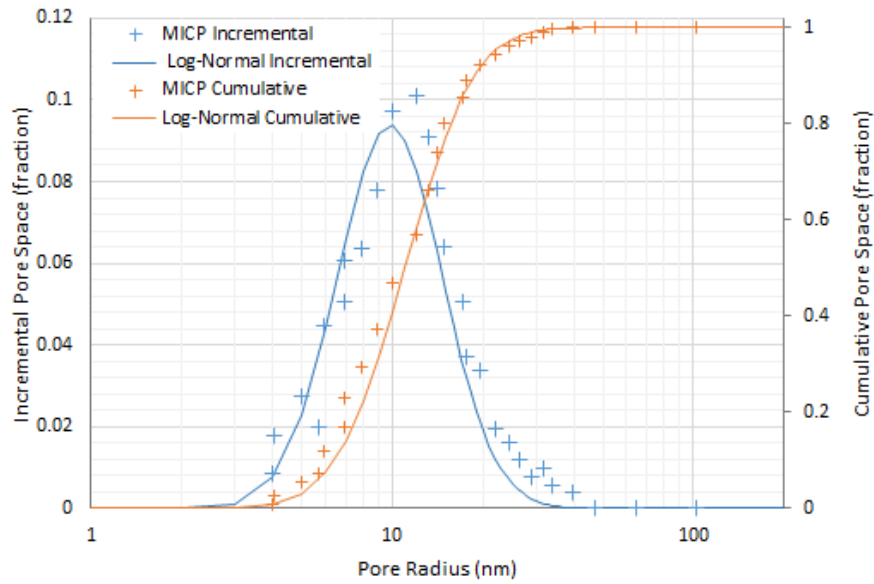
Fig. 4: Approximation of measured data of Mercury Injection Capillary Pressure (MICP) of Sample 1 to a log normal distribution $\ln N(10, 0.6)$ in terms of incremental pore space and cumulative pore space vs. pore radius.
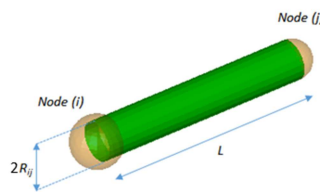
Fig. 5—Modelling a nanotube (in green) connecting two nodes (in orange)
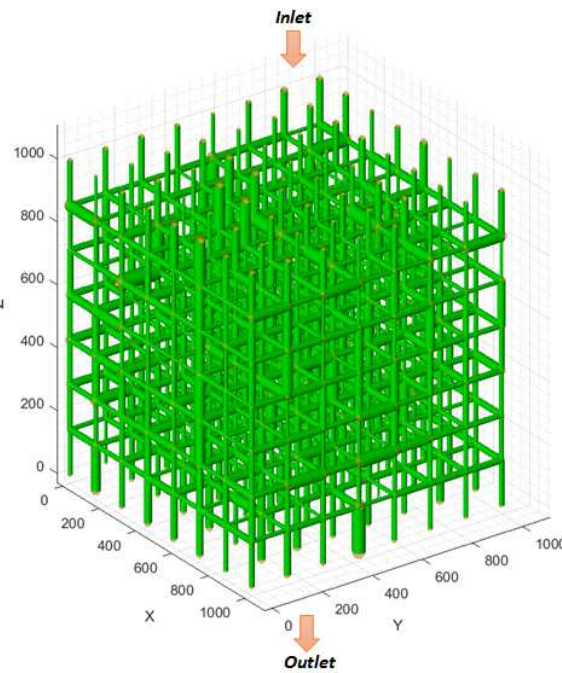
Fig. 6: Example of a 3D structure pore network with connection factor 6 and 512 nodes with inlet and outlet indicated (dimensions in nm).
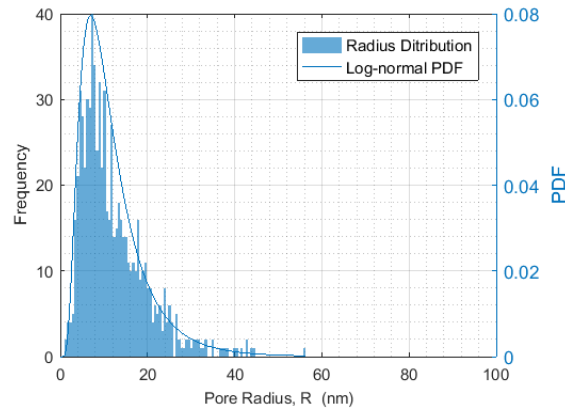
Fig. 7: Pore radius distribution of the pore network: a) Histogram of pore radius and b) PDF of $\ln N(10, 0.6)$ fitting the pore radius distribution.
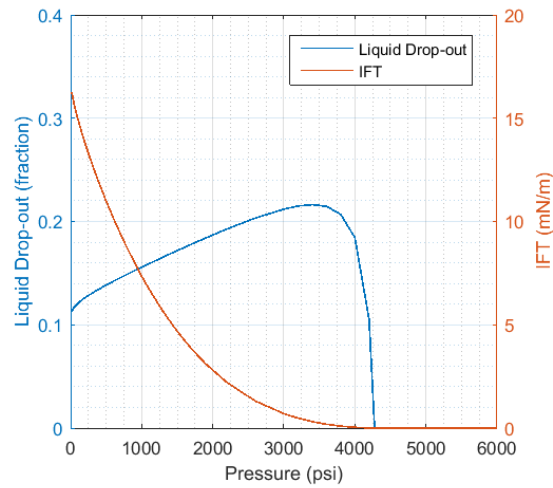
Fig. 8: Liquid Drop-out and IFT of gas condensate CVD simulation.
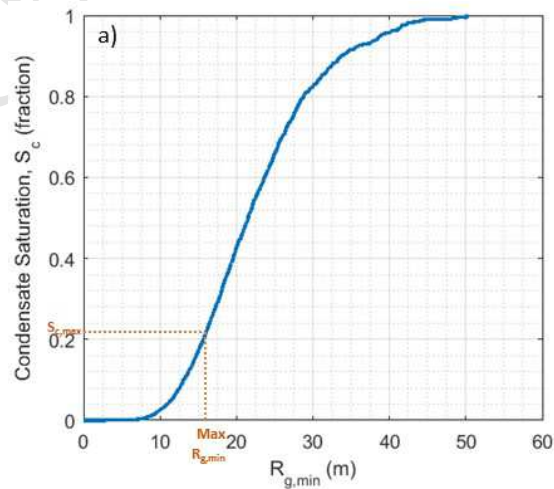
Fig. 9: Saturation function and capillary pressure a pore network of 8×8×8 nodes and $\ln \mathcal{N}(10, 0.6)$: a) Condensate saturation S_c as function of $R_{g,min}$ showing maximum condensate saturation is related to $R_{g,min}$ of 16nm, b) Capillary pressure as function of saturation and for different pressure values.
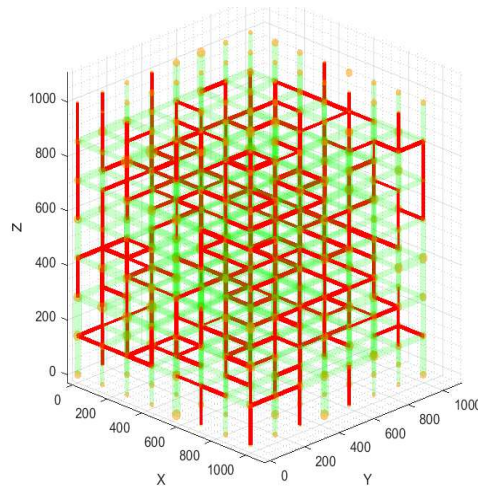
Fig. 10: An example of pore network with blocked pores in red and free pores in green at maximum condensate saturation of 22% (dimensions in nm).
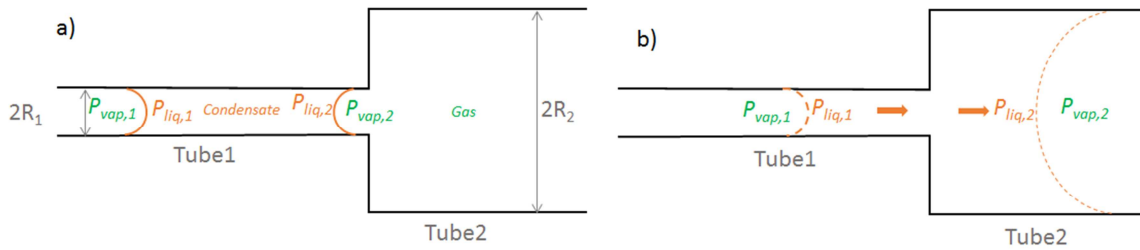
Fig. 11: Schematic of condensate flow from one nanotube to another: a) immobile condensate in Tube1, trapped by capillary pressure, b) condensate flowing from Tub1 to Tube2.

```
                        ┌─────────┐
                        │  Start  │
                        └─────────┘
                             │
                             ▼
        ┌──────────────────────────────────────────┐
        │              Input Data                    │
        ├──────────────────────────────────────────┤
        │ Pore Size Dist.: Mean (v) and Standard     │
        │ Deviation (s)                              │
        │ Network Dimensions                         │
        │ PVT Data                                   │
        │ Knudsen Flow Parameters                    │
        │ Pressure Steps Number (Pnum)               │
        └──────────────────────────────────────────┘
                             │
                             ▼
                    ┌─────────────────┐
                    │ Generate random │
                    │  pore network   │
                    └─────────────────┘
                             │
                             ▼
                    ┌─────────────────┐
                    │ Read condensate │
                    │ saturation from │
                    │    PVT Data     │
                    └─────────────────┘
                             │
                             ▼
                    ╱──────────────────╲
                   │ Identify accessible │
                   │ pores for gas flow  │
                    ╲──────────────────╱
                             │
                             ▼
                    ┌─────────────────┐
                    │   Calculate     │
                    │ individual tubes│
                    │   conductance   │
                    └─────────────────┘
                             │
                             ▼
                    ┌─────────────────┐
                    │ Derive equations│ ◄──────┐
                    │     system      │        │
                    └─────────────────┘        │
                             │                 │
                             ▼            ┌──────────┐
                    ┌─────────────────┐   │   Next   │
                    │  Newton Solver  │   │ pressure │
                    └─────────────────┘   │   step   │
                             │            └──────────┘
                             ▼                 ▲
                    ┌─────────────────┐        │
                    │     Results     │        │
                    │  Q and apparent │        │
                    │       Kg        │        │
                    └─────────────────┘        │
                             │                 │
                             ▼                 │
                    ╱──────────────────╲       │
                   │  Writing Results   │      │
                    ╲──────────────────╱       │
                             │                 │
                             ▼       No        │
                    ◇──────────────◇───────────┘
                    │ Pnum reached ?│
                    ◇──────────────◇
                             │ Yes
                             ▼
                        ┌─────────┐
                        │   End   │
                        └─────────┘
```

19
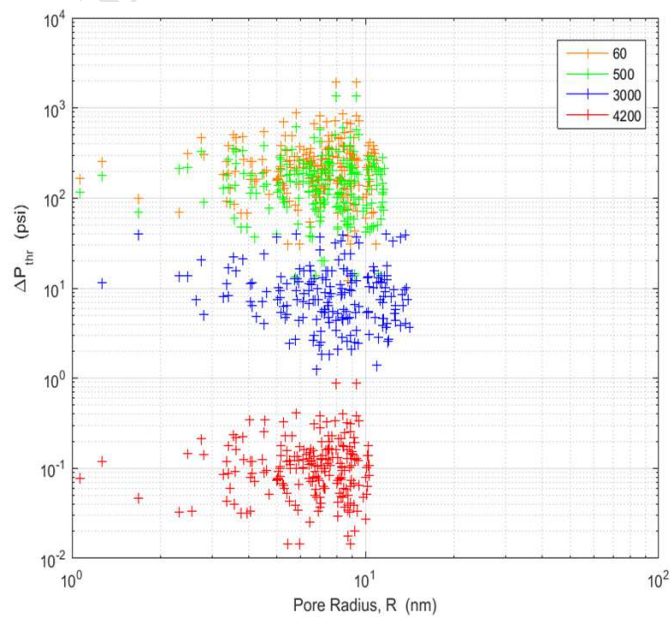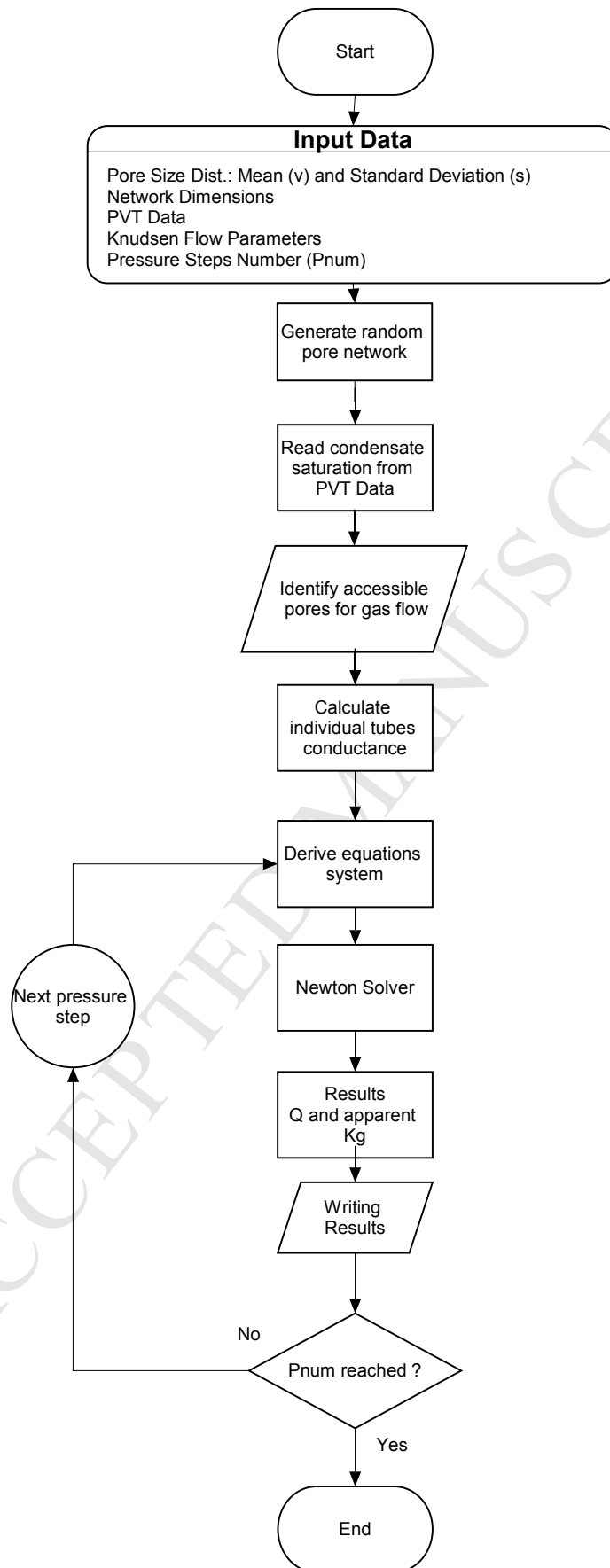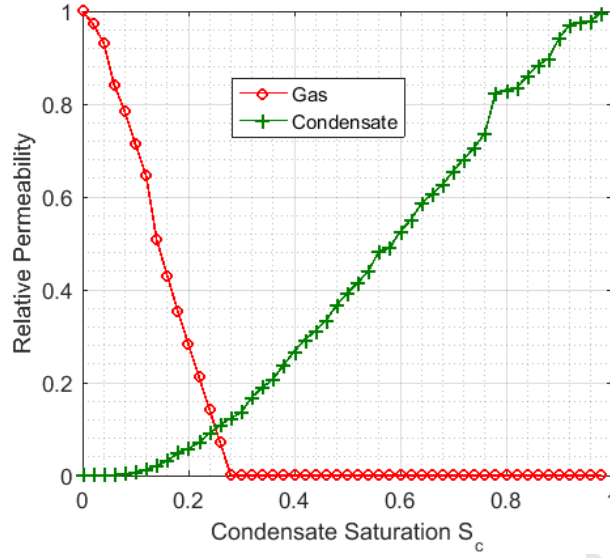
Fig. 14: Gas Darcy relative permeability and condensate relative permeability results of pore network simulation.
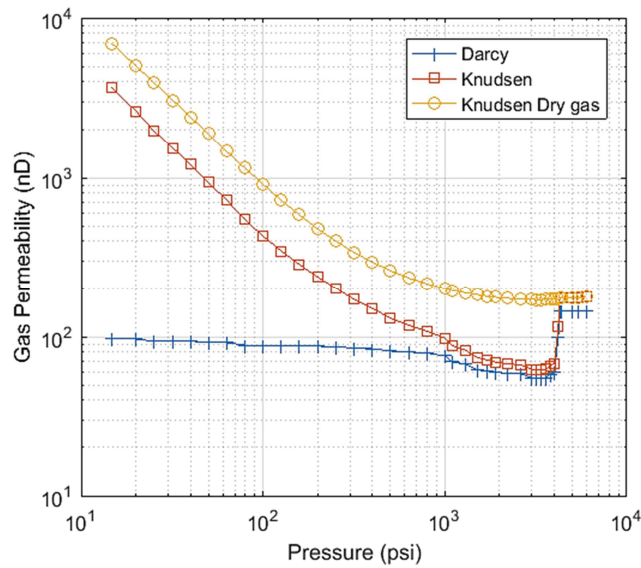
Fig. 15: Log-log plot of the pore network permeabilities Darcy flow and Knudsen flow and Knudsen dry gas flow as function of pressure for $\ln \mathcal{N}(10, 0.6)$
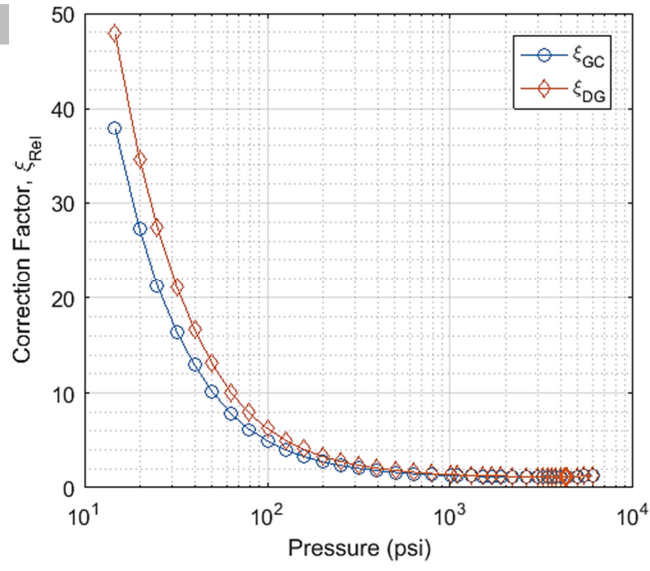
Fig. 16: Correction factors ξ_{GC} and ξ_{DG}
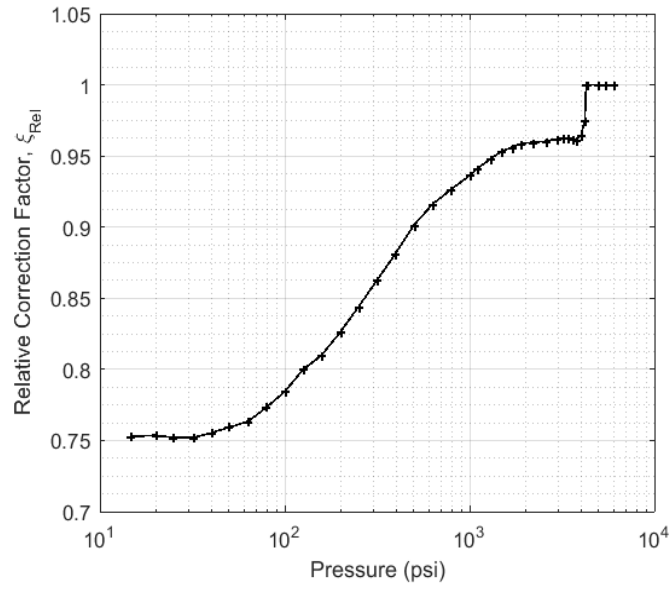
Fig. 17: Relative correction factor ξ_{rel} for pore size distribution of $\ln \mathcal{N}\,(10\,,0.6)$
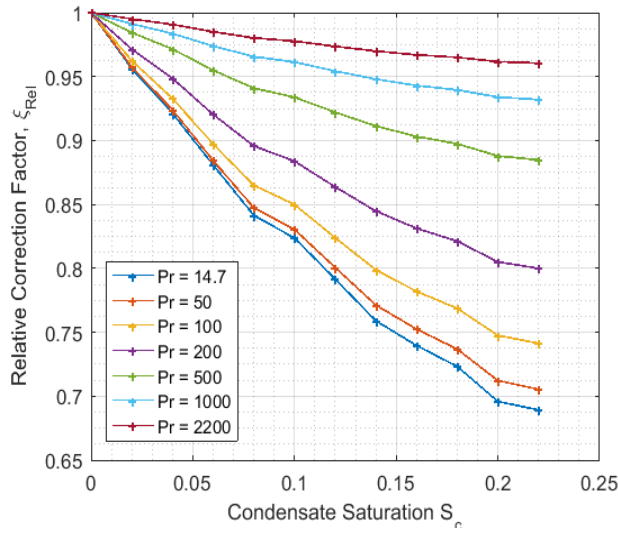
Fig. 18: ξ_{rel} vs condensate saturation for different reservoir pressures.
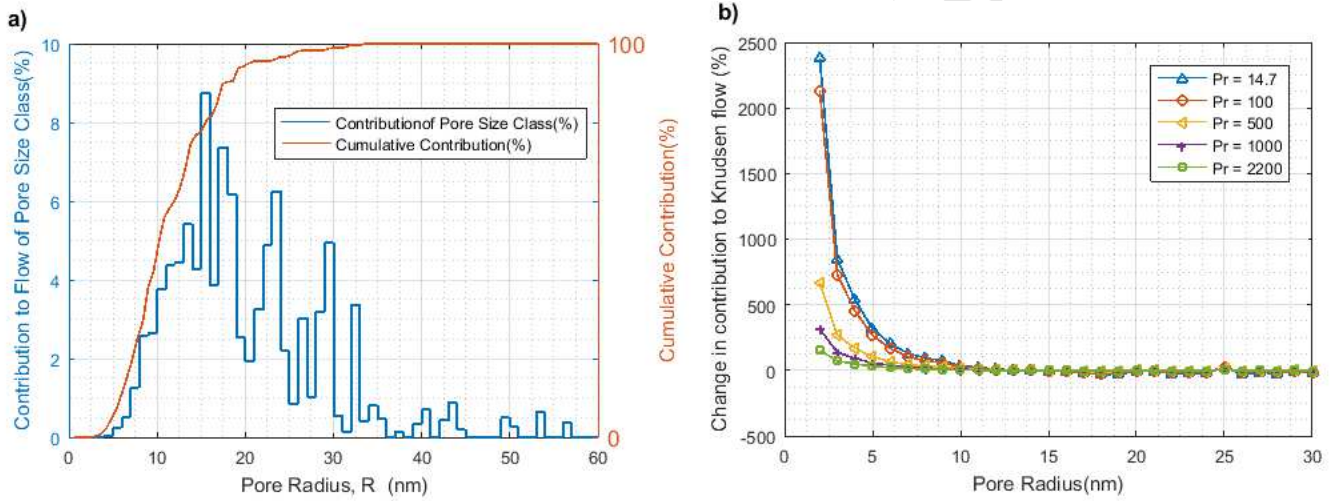
Fig. 19: Contribution of pore radius ranges to total gas flow rate for Knudsen dry gas: a) the pore size class contribution to Knudsen dry gas flow C_m^{Kn} at 2200 psi and b) the relative change of each class of pore size under Knudsen flow for different pressure values.
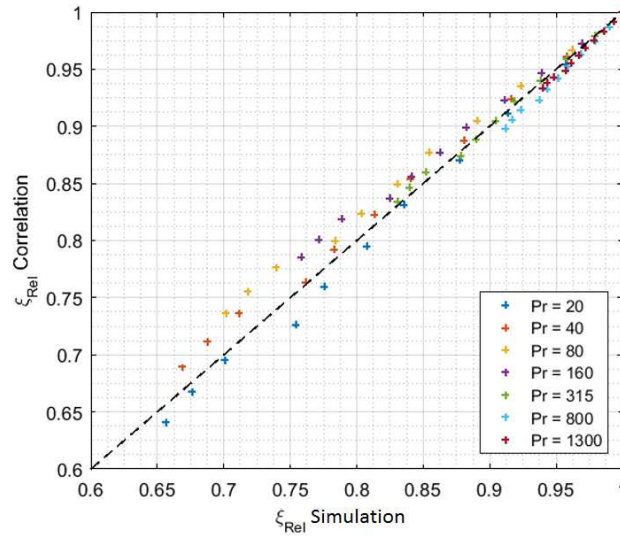
Fig. 20: Plot of ξ_{rel} values from simulation vs correlation
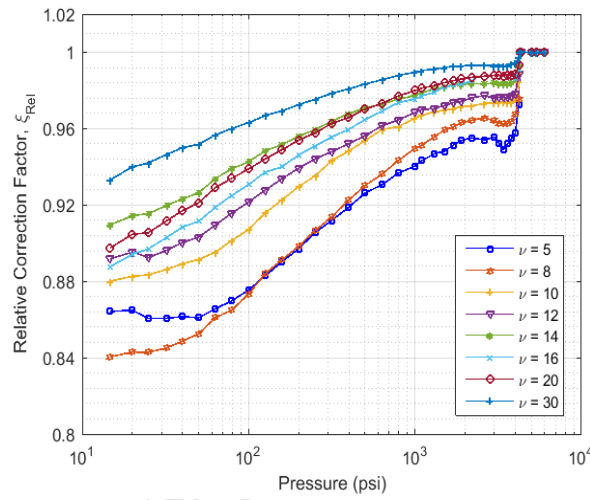
Fig. 21: Sensitivity of Relative Correction Factor ξ_{rel} to mean of pore size distribution.
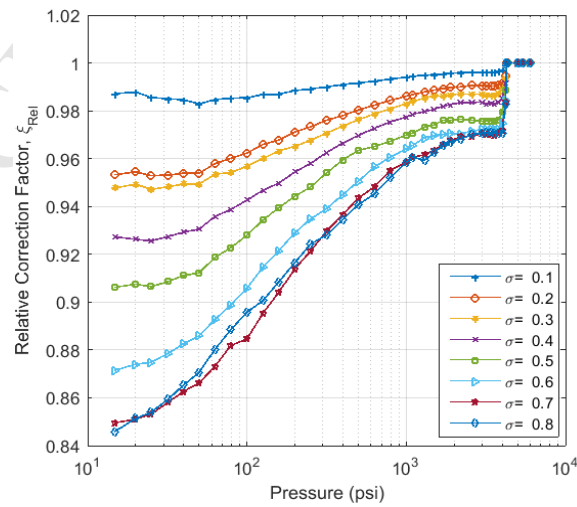
Fig. 22: Sensitivity of Relative Correction Factor ξ_{rel} to standard deviation of pore size distribution.
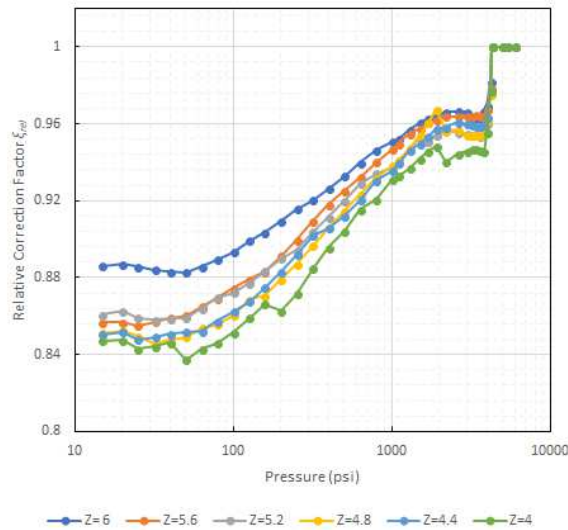
Fig. 23: Sensitivity of Relative Correction Factor ξ_{rel} to Connection number Z.

Biographies

Ismail Labed is an Assistant Professor at IPE in Heriot Watt University Dubai and he holds a PhD degree in petroleum engineering from Robert Gordon University in Aberdeen. His main research interests include flow and phase behaviour modelling of gas-condensate fluids, numerical simulation and well design optimisation in shale reservoirs. He has a professional experience as a reservoir engineer of nine years in both operator and consultancy environments. He has an extensive technical knowledge and experience in reservoir modelling and simulation, full field development and reservoir management. Ismail holds an MSc degree with Distinction in Reservoir Engineering from the Robert Gordon University and an MEng degree in Industrial Engineering from L'Ecole Nationale Polytechnique in Algiers.

Babs Oyeneyin is a Professor of Petroleum Engineering at Robert Gordon University specialising in Well Engineering, Sand Management, conventional/unconventional reservoir management and Multiphase Flow Assurance. He is a Petroleum Engineer by training and a Chartered and Registered Engineer with background in Mechanical Engineering from University of Benin. His MSc and PhD in Petroleum Engineering are from Heriot-Watt University, Edinburgh UK. For more than four decades he has initiated and worked on oilfield development projects and student-centred joint industry projects with focus on sand management, produced water and improved hydrocarbon recovery technologies. He is the founder and Chairman of the Joint Industry Sand Management Network and MD/CEO of I-Flow Solutions. He is a champion of integrated petroleum engineering solutions using a hybrid of predictive modelling and case-based reasoning with Virtual Reality Technology for real-time oilfield problem diagnosis and hydrocarbon production optimisation. His current interests are in unconventional heavy oil and shale reservoir management. Babs is a registered member of SPE and other professional bodies

Gbenga Oluyemi is a UK Chartered Engineer and a Lecturer in the School of Engineering at Robert Gordon University, Aberdeen UK. His main research interests are in petroleum geomechanics, oilfield chemistry, uncertainty modelling and production optimisation from both conventional and non-conventional reservoirs. He has more than 15 years of experience across oil and gas industry, water and environmental engineering and academia. He is currently the editor-in-chief of the Springer Petroleum Engineering Book Series. He holds PhD and MSc degrees from Robert Gordon University and a BSc degree from University of Ibadan, Nigeria.

Highlights

- A new parameter was introduced: "Relative Correction Factor" (ξ_{rel}) for gas relative permeability

- ξ_{rel} is a function of condensate saturation and pressure

- ξ_{rel} can be formulated as

$$\xi_{rel} = 1 - \frac{a}{P^b}\,(S_c)^n$$

where n, a and b are parameters of the pore size distribution.

- At high condensate saturations, Knudsen flow has insignificant effect

- The effect of condensate blockage is highly dependent on the pore size distribution.